Biomaterials 53 (2015) 229–238

Contents lists available at ScienceDirect

Biomaterials

journal homepage: www.elsevier.com/locate/biomaterials

A near-infrared phthalocyanine dye-labeled agent for integrin αvβ6-targeted theranostics of pancreatic cancer

Duo Gao [a], Liquan Gao [a], Chenran Zhang [a], Hao Liu [a], Bing Jia [a], Zhaohui Zhu [b], Fan Wang [a, c], Zhaofei Liu [a, *]

[a] Medical Isotopes Research Center and Department of Radiation Medicine, School of Basic Medical Sciences, Peking University, Beijing 100191, China
[b] Department of Nuclear Medicine, Peking Union Medical College Hospital, Beijing 100857, China
[c] Interdisciplinary Laboratory, Institute of Biophysics, Chinese Academy of Sciences, Beijing 100101, China

chinaXiv:201605.01329v1

ARTICLE INFO

Article history:
Received 2 December 2014
Received in revised form
17 February 2015
Accepted 21 February 2015
Available online 14 March 2015

Keywords:
Molecular imaging
Intraoperative imaging
Molecular probe
Image-guided surgery
Photodynamic therapy

ABSTRACT

Integrin αvβ6 is widely upregulated in variant malignant cancers but is undetectable in normal organs, making it a promising target for cancer diagnostic imaging and therapy. Using streptavidin-biotin chemistry, we synthesized an integrin αvβ6-targeted near-infrared phthalocyanine dye-labeled agent, termed Dye-SA-B-HK, and investigated whether it could be used for cancer imaging, optical imaging-guided surgery, and phototherapy in pancreatic cancer mouse models. Dye-SA-B-HK specifically bound to integrin αvβ6 in vitro and in vivo with high receptor binding affinity. Using small-animal optical imaging, we detected subcutaneous and orthotopic BxPC-3 human pancreatic cancer xenografts in vivo. Upon optical image-guidance, the orthotopically growing pancreatic cancer lesions could be successfully removed by surgery. Using light irradiation, Dye-SA-B-HK manifested remarkable antitumor effects both in vitro and in vivo. ^{18}F-FDG positron emission tomography (PET) imaging and ex vivo fluorescence staining validated the observed decrease in proliferation of treated tumors by Dye-DA-B-HK phototherapy. Tissue microarray results revealed overexpression of integrin αvβ6 in over 95% cases of human pancreatic cancer, indicating that theranostic application of Dye-DA-B-HK has clear translational potential. Overall, the results of this study demonstrated that integrin αvβ6-specific Dye-SA-B-HK is a promising theranostic agent for the management of pancreatic cancer.

© 2015 Elsevier Ltd. All rights reserved.

1. Introduction

Pancreatic cancer ranks as the fourth most common cause of cancer-related deaths in developed countries and is characterized by resistance to conventional therapies such as chemo- and radiotherapy [1,2]. Systemic therapies are nearly ineffective in advanced pancreatic cancer, and prognosis for patients is extremely poor, with a five-year survival rate generally below 5% [1,3]. Because of the high mortality and rapid progression associated with pancreatic cancer, the best approach for disease management involves early detection and accurate staging. Currently, most pancreatic cancer patients are diagnosed at advanced stages, and the standard care (surgical resection followed by adjuvant therapy) is only partially effective in patients diagnosed at early stages [2]. Therefore, early diagnosis, accurate staging, and the development of more effective strategies to treat pancreatic cancer are critical for improving patient care.

Advances in molecular imaging approaches including positron emission tomography (PET), single-photon emission computed tomography (SPECT), molecular magnetic resonance (mMRI), optical imaging, and targeted ultrasound imaging have offered opportunities for significantly improving cancer management through early detection of lesions, patient stratification for therapies, treatment monitoring, image-guided therapy, and surgical guidance during tumor resection. Among the imaging modalities, optical imaging has the advantages of non-requirement of ionizing radiation and low cost. Importantly, optical imaging can be tumor-specific and offers superior resolution and sensitivity, an inherent advantage for surgical inspection and practice. Recently, the first human application of intraoperative tumor-specific optical imaging for real-time visualization of tumor lesions in ovarian cancer patients has been reported [4]. Accurate real-time imaging using tumor-specific fluorescent agents (probes) enables localization of tumor lesions that are difficult or impossible to be detected by gross

* Corresponding author. Tel./fax: +86 10 82802871.
E-mail address: liuzf@bjmu.edu.cn (Z. Liu).

http://dx.doi.org/10.1016/j.biomaterials.2015.02.093
0142-9612/© 2015 Elsevier Ltd. All rights reserved.

observation, which allows for more accurate excision of tumor lesions.

Near-infrared (NIR) fluorescence imaging takes advantage of NIR dye-labeled agents with wavelengths of 700–900 nm range, a range in which tissue autofluorescence is minimal, allowing for favorable tissue penetration and high target-to-background contrast [5,6]. Moreover, certain NIR dyes, such as the phthalocyanine dye IRDye700, can also serve as photosensitizers for potential cancer photodynamic therapy (PDT) [7]. PDT, which is a minor invasive treatment strategy that has potential use for various diseases, can destroy abnormal tissue by administration of a photosensitizer followed by irradiation with light at a wavelength corresponding to the absorbance band of the sensitizer [8,9]. Although a promising approach, PDT has limited use in cancer therapy because non-targeted photosensitizers can also non-specifically accumulate in normal organs, producing severe side effects [10]. To increase the selectivity of photosensitizers in tumors, pioneering work has been done by the Kobayashi group, which developed a series of antibody-photosensitizer conjugates for cancer antigen targeted PDT that has been called photoimmunotherapy (PIT) [11–13]. The antibody-photosensitizer conjugate-based tumor PIT showed significantly improved antitumor effect compared with the non-specific PDT, demonstrating that the specific delivery of photosensitizers can significantly increase tumor selectivity and improve therapy efficacy.

PIT using a monoclonal antibody as the delivery vehicle for pancreatic cancer may have limitations. These include high accumulation of intact antibody in the liver, which is adjacent to the pancreas, due to hepatic clearance of large molecular weight molecules [14]. The results may lead to severe liver toxicity following light irradiation. In contrast to antibody, peptide has low molecular weight, fast blood clearance, and rapid tissue penetration. Recently, we have developed a ^{99m}Tc radiolabeled linear peptide (^{99m}Tc-labeled HK peptide; ^{99m}Tc-HHK) for SPECT detection of pancreatic cancer by targeting integrin αvβ6 [15], which is overexpressed in pancreatic cancer but is negligibly expressed in normal tissues [16,17]. ^{99m}Tc-HHK exhibited high αvβ6 selectivity and could specifically detect liver metastatic lesions of integrin αvβ6-positive tumors [15]. However, a major drawback of ^{99m}Tc-HHK is its relatively low tumor uptake, which could be partly due to its low integrin αvβ6-binding affinity, as it is a linear peptide that is monovalent with respect to receptor binding.

In this study, we prepared an integrin αvβ6-targeting agent using streptavidin-biotin chemistry, which is expected to be multivalent for receptor targeting. The targeting agent was labeled with an NIR photosensitizer IRDye700 and tested in animal models for integrin αvβ6-targeted optical imaging of pancreatic cancer, image-guided surgery of orthotopic pancreatic cancer tissue, and tumor-targeted phototherapy (PT).

2. Materials and methods

2.1. General remarks

All commercially obtained chemicals were of analytic grade and used without further purification. The integrin αvβ6-specific peptides Fmoc-protected RGDLATLRQLAQEDGVVGVRK (Fmoc-HK; H means H2009.1, the denoted name of the underlined peptide sequence [18]) and RGDLATLRQLAQEDGVVGVRYK (HYK) were synthesized as previously described [15]. Na^{125}I was purchased from Perkin–Elmer (Waltham, MA, USA). The reversed-phase high-performance liquid chromatography (HPLC) system was the same as previously reported [15].

2.2. Synthesis of phthalocyanine dye-labeled agent dye-SA-B-HK

A solution of 2 μmol Fmoc-HK was mixed with 3 μmol of biotin-X-NHS ester (water-soluble, Millipore, Billerica, MA, USA) in 500 μL of 0.1 M sodium bicarbonate buffer (pH 8.5). After stirring for 2 h at room temperature, Fmoc-HK-biotin-X was isolated by semi-preparative HPLC. The fraction containing the product was collected and lyophilized. Fmoc-HK-biotin-X was obtained in 43% yield with >95% purity. After removal of the Fmoc group with 20% piperidine in dimethylformamide, the final HK-biotin-X (B-HK) product was generated. Analytical HPLC and mass spectrometry analyses were performed to identify the product.

Dye-labeled streptavidin was generated using a previously described method [19,20]. Briefly, 5 mg streptavidin was mixed with the IRDye700DX *N*-hydroxysuccinimide ester (LI-COR, Inc. Lincoln, NE, USA) at a mole ratio of 1: 7 in 0.1 M sodium bicarbonate buffer (pH 8.3). After 1 h incubation at room temperature, IRDye700-streptavidin (Dye-SA) product was purified using a PD-10 desalting column (GE Healthcare, Piscataway, NJ, USA) and concentrated by Centricon filter (Millipore, Bedford, MA, USA). The degree of labeling (dye/protein ratio) for Dye-SA was calculated to be approximately 3.8 based on UV measurements. A solution of Dye-SA was then mixed with excess amounts of B-HK to occupy all streptavidin binding sites. After stirring for 20 min at room temperature, unbound B-HK was removed using a PD-10 desalting column with phosphate-buffered saline (PBS) as the mobile phase and the final product termed Dye-SA-B-HK (Fig. 1A) was obtained. The control agent Dye-streptavidin-biotin (Dye-SA-B) without the targeting peptide was also prepared using similar procedure.

2.3. Cell culture and animal models

The BxPC-3 human pancreatic cancer cell line was obtained from American Type Culture Collection. Tumor cells were grown in RPMI-1640 medium supplemented with 10% fetal bovine serum (FBS) at 37 °C in humidified atmosphere containing 5% CO_2.

All animal experiments were performed in accordance with the guidelines of Peking University Animal Care and Use Committee. To establish the BxPC-3 subcutaneous tumor model, BxPC-3 cells (1×10^7 in 100 μL of PBS) were inoculated subcutaneously into the upper right (for imaging studies) or both right and left (for therapeutic studies) upper flanks of male BALB/c nude mice (5–6 weeks of age; Department of Laboratory Animal Science, Peking University, Beijing, China). For the establishment of an orthotopic human pancreatic cancer mouse model, mice were anesthetized by inhalation of 2% isoflurane in oxygen. A small incision was made in the left abdomen of each mouse and the spleen was carefully exposed by a gentle pull. BxPC-3 cells (5×10^6) in 50 μL of PBS were then slowly injected into the pancreas tissue in an area adjacent to the spleen. Upon completion, the spleen was returned to the abdomen and the incision was closed using sutures. Mice were used for small-animal fluorescence imaging studies approximately 30 days after cell injection (based on our pilot data).

2.4. Cell competitive binding assay

The in vitro integrin αvβ6-binding affinity of Dye-SA-B-HK was compared with the HK peptide under exactly the same experimental conditions via a cellular displacement assay using ^{125}I-HYK as the integrin αvβ6-specific radioligand. ^{125}I-HYK was prepared by labeling the HYK peptide with Na^{125}I using the Iodogen method [21]. The experiments were performed on BxPC-3 cells using a previously described method [15]. The best-fit 50% inhibitory concentration (IC_{50}) values were calculated by fitting the data with nonlinear regression using Prism software (version 5.0; GraphPad Software, Inc. San Diego, CA, USA). Experiments were performed twice using quadruple samples.

2.5. Cell staining

The BxPC-3 cells grown on 35 mm MatTek glass-bottom culture dishes were incubated with Dye-SA-B-HK or Dye-SA-B (100 nmol/L in PBS) for 1 h at room temperature. Integrin αvβ6-binding specificity of Dye-SA-B-HK was verified by incubating BxPC-3 cells with a blocking dose of the non-fluorescent HK peptide (10 μmol/L). Post incubation, cells were washed with PBS and visualized using a confocal microscope.

2.6. In vivo optical imaging

The in vivo behavior of Dye-SA-B-HK was evaluated in five BxPC-3 tumor-bearing nude mice. Each animal was injected via the tail vein with 0.5 nmol of Dye-SA-B-HK. At 1, 2, 4, 8, and 24 h postinjection (p.i.), the mice were anesthetized by inhalation of 2% isoflurane in oxygen and then subjected to optical imaging using a Maestro In-Vivo Imaging System (CRI, Woburn, MA, USA). For each scan, aliquots containing a known amount of injectate were placed on the black papers and were subjected to optical imaging together with the mice. Identical illumination settings were used to obtain all scans. Images were acquired and analyzed using Maestro 2.4 software (CRI, Woburn, MA, USA). The fluorescence intensity was presented as the average radiant efficiency in the unit of [p/sec/cm^2/sr]/[μW/cm^2]. Tumor uptake was calculated by normalizing the tumor fluorescence intensity by the total injection dose. To determine the tumor targeting specificity of Dye-SA-B-HK, three groups of mice ($n = 5$ per group) were intravenously (i.v.) injected with 0.5 nmol Dye-SA-B-HK, the mixture composed of 500 μg HK peptide and 0.5 nmol Dye-SA-B-HK, and 0.5 nmol Dye-SA-B, respectively. At 2 h p.i., mice were subjected to optical imaging using the same protocol.

For the optical imaging-guided surgery, mice bearing orthotopic BxPC-3 pancreatic cancer xenografts were i.v. injected with 0.5 nmol Dye-SA-B-HK. Mice were anesthetized and optical imaging was performed at 2 h p.i. using an IVIS small-animal imaging system (Xenogen, Alameda, CA, USA). After in vivo imaging, mice

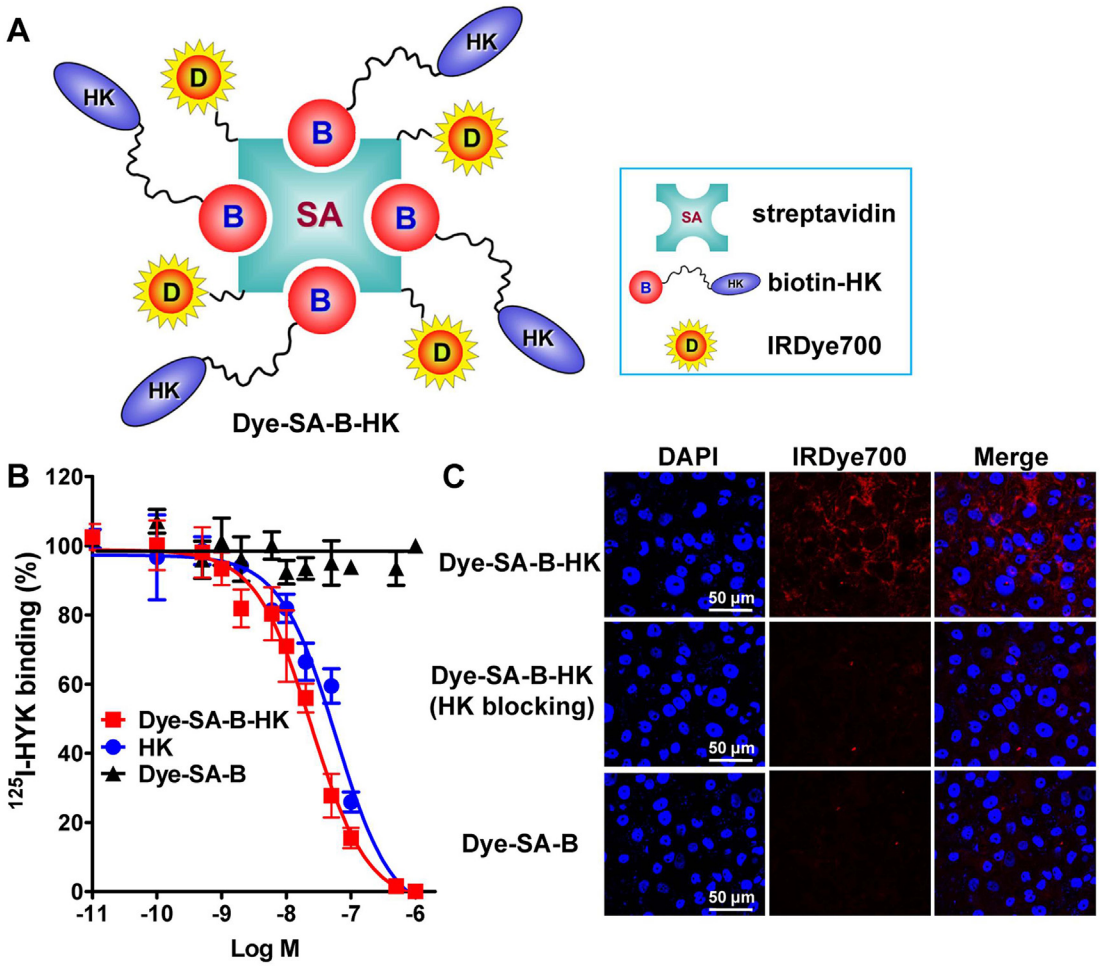

Fig. 1. (A) Schematic drawing of the integrin αvβ6-targeting near-infrared fluorescence agent, Dye-SA-B-HK. (B) Inhibition of ^{125}I-HYK binding to integrin αvβ6 on BxPC-3 tumor cells by Dye-SA-B-HK, HK peptide, and Dye-SA-B. Data are shown as mean ± SD (n = 4). (C) Fluorescence staining of the integrin αvβ6-positive BxPC-3 tumor cells using Dye-SA-B-HK (with or without a blocking concentration of the HK peptide) or Dye-SA-B.

were sacrificed and surgery was performed to resect the tumor nodules. Optical imaging was subsequently repeated to check the residual tumor tissues. For further confirmation of the orthotopic tumor lesions in the pancreas, surgically excised tumor lesions were fixed in 5% buffered formalin, embedded in paraffin, cut into sections, and subjected to hematoxylin and eosin (H&E) staining.

2.7. Intratumoral distribution of dye-SA-B-HK

To determine the intratumoral microdistribution of Dye-SA-B-HK, a subset of surgically removed orthotopic tumors were immediately frozen in OCT medium and cut into 5-μm-thick slices. After fixation with ice-cold acetone, rinsing with PBS and blocking with 10% FBS for 30 min at room temperature, tumor sections were incubated with mouse anti-human integrin αvβ6 monoclonal antibody (Millipore, Billerica, MA, USA) for 1 h at room temperature and visualized using FITC-conjugated secondary antibody (Jackson ImmunoResearch Laboratories, Inc., West Grove, CA, USA) using a confocal microscope.

2.8. In vitro and in vivo PT studies

The BxPC-3 cells were seeded in 35 mm MatTek glass-bottom culture dishes (1×10^4 per dish) and incubated overnight at 37 °C to allow adherence. After changing with fresh culture medium, cells were incubated with PBS, Dye-SA-B (100 nmol/L in PBS), or Dye-SA-B-HK (100 nmol/L in PBS) for 2 h at 37 °C. Afterward, cells were washed with PBS and then either untreated or exposed to 690 nm light irradiation under the calculated doses of 2 and 4 J/cm^2, respectively. After treatment, cells were stained with a Necrosis Detection Kit (Abcam Inc., Cambridge, MA, USA) and analyzed using a confocal microscope. Experiments were performed twice using five parallel samples.

To assess the therapeutic efficacy of integrin αvβ6-targeted PT in vivo, nude mice bearing BxPC-3 cancer xenografts in both right and left front flanks with a uniform tumor size of ~100 mm^3 were chosen and segregated into three groups: PBS control, Dye-SA-B, and Dye-SA-B-HK groups (n = 15 per group). Each mouse was injected via tail vein with four doses of PBS, Dye-SA-B (1.0 nmol), or Dye-SA-B-HK (1.0 nmol) on days 0, 3, 7, and 10, respectively. Light irradiation (35 J/cm^2) was conducted exclusively on the right side of the tumor of all mice from the Dye-SA-B and Dye-SA-B-HK groups 2 h after each injection. Tumor size and body weight were measured every other day. The tumor volume was calculated using the formula volume = length × width^2/2. Five mice from each group were subjected to small-animal ^{18}F-FDG PET imaging on day 11 (see timeline of the PT and PET imaging experiments in Fig. 4C).

2.9. Small-animal PET imaging

Small-animal ^{18}F-FDG PET imaging was performed using a microPET R4 rodent model scanner (Siemens Medical Solutions, Erlangen, Germany). Mice were injected i.v. with 3.7 MBq (100 μCi) of ^{18}F-FDG. Five-min static PET scans were acquired at 1 h p.i. The images were reconstructed by a two-dimensional ordered-subsets expectation maximum (OSEM) algorithm, and the region-of-interests–derived %ID/g values were calculated as previously described [15,22]. Immediately after the PET scans, mice were sacrificed, and tumors were excised and frozen in OCT medium, then cut into 5-μm-thick slices for immunofluorescence staining.

2.10. Immunofluorescence staining

Immunofluorescence staining studies were performed to quantify GLUT-1 and Ki67 in tumor tissues with or without the treatment of Dye-SA-B or Dye-SA-B-HK PT. Tumor slices were incubated with anti-GLUT-1 and anti-Ki67 (Millipore, Billerica, MA, USA) primary antibodies, respectively. The slices were then visualized using Cy3-conjugated secondary antibodies (Jackson ImmunoResearch Laboratories, West Grove, PA, USA) under a confocal microscope.

2.11. Tissue microarray of human pancreatic cancers

To determine whether integrin αvβ6 is widely expressed in human pancreatic cancer, a tissue microarray (TMA) experiment was performed. Tumor tissue specimens randomly obtained from 90 patients with pancreatic cancer were selected for TMA construction (collaborated with the Shanghai Biochip Company Ltd., Shanghai, China) using a well-established method [23]. The TMA slide was next subjected to standard immunohistochemistry using an anti-integrin αvβ6 primary antibody (1: 500; Bioss, Inc. Beijing, China). Staining results were quantified from tumor TMA cores, using a four-value membrane score by an experienced pathologist who was blinded. Scores of 0 and 1 were considered negative for integrin αvβ6, whereas scores of 2 and 3 were considered positive [24].

2.12. Statistical analysis

Quantitative data are expressed as means ± SD. Means were compared using one-way analysis of variance (ANOVA) and Student's t test. P values <0.05 were considered statistically significant.

3. Results

3.1. Synthesis and in vitro characterization of dye-SA-B-HK

The integrin αvβ6-targeting fluorescence imaging agent Dye-SA-B-HK was synthesized using streptavidin-biotin binding chemistry (Fig. 1A). The identity of biotinylated HK peptide (B-HK) was confirmed by both analytical HPLC (Rt = 16.87 min) and mass spectrometry (MALDI-TOF-MS: m/z, 2620.20) analyses.

The receptor-binding affinity of Dye-SA-B-HK was compared with that of the HK peptide by performing a competitive displacement assay with ^{125}I-HYK (integrin αvβ6 specific) as the radioligand. Dye-SA-B was also added for comparison. As shown in Fig. 1B, Dye-SA-B-HK and HK inhibited binding of ^{125}I-HYK to integrin αvβ6-positive BxPC-3 cells in a concentration-dependent manner. The IC_{50} values for Dye-SA-B-HK and HK were determined to be $(2.45 \pm 1.68) \times 10^{-8}$ M and $(5.84 \pm 1.52) \times 10^{-8}$ M, respectively. Dye-SA-B did not show significant binding inhibition of ^{125}I-HYK. The IC_{50} values of the compounds suggest that the streptavidin-biotin strategy significantly increased receptor-binding affinity of Dye-SA-B-HK compared with HK peptide ($P < 0.05$).

Direct staining of BxPC-3 tumor cells using Dye-SA-B-HK was performed to further determine in vitro tumor specificity. As shown in Fig. 1C, BxPC-3 cells incubated with Dye-SA-B-HK exhibited strong staining whereas the Dye-SA-B conjugate without the targeting peptide did not bind the BxPC-3 cells. In the presence of an excess dose of non-fluorescent HK peptide, BxPC-3 cells incubated with Dye-SA-B-HK exhibited no staining (Fig. 1C), further confirming integrin αvβ6-binding specificity.

3.2. In vivo integrin αvβ6-targeting of dye-SA-B-HK

The in vivo tumor-targeting efficacy of Dye-SA-B-HK was investigated in BxPC-3 tumor-bearing nude mice using the small-animal in vivo optical imaging system. The tumor accumulation of Dye-SA-B-HK was clearly visualized from 1 to 24 h p.i. (Fig. 2A). The region of interest (ROI) was drawn for each tumor or muscle over time, and the total signal was normalized by the exposure time and tumor size. Dye-SA-B-HK showed the highest % fluorescence intensity in the tumor at 1 h p.i. (2.91 ± 0.34%), and then significantly decreased at 4 (2.28 ± 0.25%; $P < 0.05$), 8 (2.26 ± 0.39%; $P < 0.05$), and 24 (1.62 ± 0.28%; $P < 0.01$) p.i. (Fig. 2B). The light intensity ratios between the tumor and muscle (tumor/muscle ratio) for Dye-SA-B-HK were calculated at each time point. As shown in Fig. 2C, Dye-SA-B-HK had significantly increased tumor-to-muscle ratios from 1 to 8 h (2.43 ± 0.42 vs. 2.96 ± 0.37; $P < 0.05$), and then maintained the high level up to 24 h.

The tumor-targeting specificity of Dye-SA-B-HK in vivo was confirmed by a blocking study. As shown in Fig. 2D and E, the tumor uptake of Dye-SA-B-HK at 2 h p.i. was significantly inhibited by co-injection of an excess dose of HK peptide (2.72 ± 0.17% vs. 0.56 ± 0.04%; $P < 0.001$). The tumor uptake (1.45 ± 0.21%) of Dye-SA-B at 2 h p.i. was also significantly lower than that of Dye-SA-B-HK ($P < 0.01$). These results demonstrated the specific in vivo targeting of Dye-SA-B-HK in BxPC-3 tumors.

3.3. Dye-SA-B-HK optical imaging-guided surgery

Preoperative optical imaging using Dye-SA-B-HK was performed to investigate whether the technique could be used for fluorescence image-guided surgery on mice bearing orthotopically growing pancreatic cancer xenografts. After whole body optical imaging, strong fluorescence signal was detected in the left abdominal region. Under the guidance of optical imaging, the tumors were successfully removed by surgery. Optical imaging after surgery confirmed complete removal of the tumor lesions (Fig. 3A). The removed tumor tissues were subjected to histology examination. The H&E staining results of the dissected tumor lesion further confirmed the presence of tumor lesions adjacent to the normal pancreatic tissues (Fig. 3B).

3.4. Intratumoral microdistribution of dye-SA-B-HK

To characterize the microdistribution of Dye-SA-B-HK in orthotopically growing BxPC-3 tumors, the surgically-removed tumor tissue was frozen cut, and tumor sections were stained using an anti-human integrin αvβ6 antibody to localize the integrin αvβ6 expression. As shown in Fig. 3C, BxPC-3 tumor tissues stained positively for human integrin αvβ6. Overlying imaging revealed that most of the Dye-SA-B-HK positive area co-expressed human integrin αvβ6 (Fig. 3D), demonstrating the integrin αvβ6-specific localization of Dye-SA-B-HK in BxPC-3 tumor tissues.

3.5. In vitro and in vivo PT using dye-SA-B-HK

To determine the PT effect of Dye-SA-B-HK, we first investigated its cell killing capacity in vitro. Live and necrotic cell fluorescence staining showed integrin αvβ6-specific induction of cell necrosis (Fig. 4A). Compared with control groups, PT of Dye-SA-B-HK demonstrated evident tumor cell toxicity. PT also showed light irradiation dose dependence, as evidenced by a significantly increased tumor necrosis fraction in the 4 J/cm^2 group compared with the 2 J/cm^2 group (17.89 ± 1.83% vs. 10.85 ± 0.78%; $P < 0.01$) (Fig. 4B).

We next investigated the in vivo tumor therapy efficacy of Dye-SA-B-HK-based PT in the integrin αvβ6-positive BxPC-3 tumor model. As shown in Fig. 4C, a time-dependent increase in tumor volume was observed in the PBS and non-irradiated groups (Dye-SA-B and Dye-SA-B-HK). In contrast, four doses of Dye-SA-B-HK irradiation significantly inhibited tumor growth on day 24 compared with control groups. On day 34, the average volumes were 1914.63 ± 291.64, 1559.27 ± 500.54, 1107.70 ± 189.11, 1418.06 ± 122.68, and 590.54 ± 300.02 mm^3 for the PBS, Dye-A-B, Dye-A-B PT, Dye-A-B-HK, and Dye-A-B-HK PT groups, respectively. Although the Dye-SA-B-HK phototherapy group exhibited evident antitumor effect, we observed neither mortality nor noticeable body weight loss among the treated mice (Fig. 4D). These results suggest Dye-SA-B-HK-based PT had no over toxicity in mice.

3.6. Therapy response monitoring using PET

To determine the tumor therapy response of Dye-SA-B-HK PT in the BxPC-3 tumors, we performed ^{18}F-FDG PET imaging studies to quantify tumor cell glucose metabolism. As shown in Fig. 5A, the

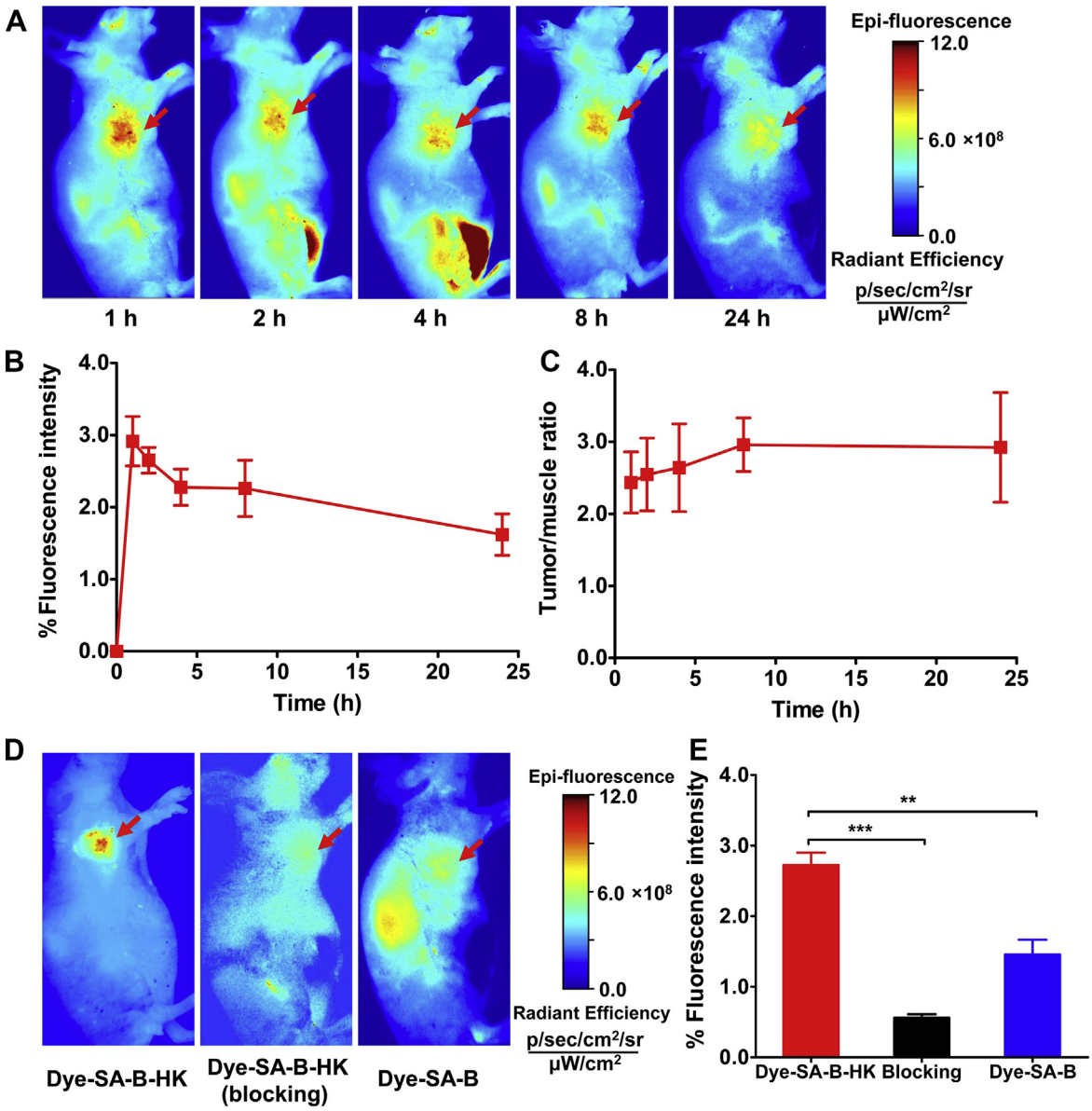

Fig. 2. (A) Representative near-infrared fluorescence sagittal images of Dye-SA-B-HK in BxPC-3 tumor-bearing nude mice at 1, 2, 4, 8, and 24 h postinjection. (B–C) Quantified in vivo tumor uptake (B) and tumor-to-muscle ratios (C) of Dye-SA-B-HK in BxPC-3 tumor-bearing nude mice. Results are expressed as mean ± SD (n = 5). (D–E) In vivo near-infrared fluorescence sagittal imaging (D) and quantified tumor uptake (E) of BxPC-3 tumor-bearing nude mice at 2 h after intravenous injection of Dye-SA-B-HK (with or without the blocking of an excess dose of the HK peptide) or Dye-SA-B. Results are expressed as mean ± SD (n = 5 per group). **, $P < 0.01$; ***, $P < 0.001$. Arrows indicate the tumors in all cases.

BxPC-3 tumors were clearly visualized with good tumor-to-background ratio for the PBS and non-phototherapy groups. The uptake in the tumor was measured from the ROI analysis. The quantified tumor uptake of ^{18}F-FDG in the Dye-SA-B-HK PT group was significantly lower than PBS, Dye-SA-B only, Dye-SA-B PT, or the Dye-SA-B-HK-only group ($P < 0.01$) (Fig. 5B).

3.7. Immunofluorescence staining

To further confirm the in vivo PET imaging results, we also performed ex vivo immunofluorescence staining to determine the tumor GLUT-1 and Ki67 levels, markers reflecting tumor glucose metabolism and cell DNA synthesis, respectively. As shown in Fig. 5C and D, tumor tissue fluorescence staining showed decreased GLUT-1 and Ki67 expression in the Dye-SA-B-HK PT-treated tumors, whereas BxPC-3 tumors in other groups had similar glucose metabolic activity and an equivalent cell proliferation index.

3.8. Human pancreatic cancer TMA

We performed a human pancreatic cancer TMA to determine whether integrin αvβ6 is overexpressed in human pancreatic cancer lesions. Tumor tissue specimens were randomly obtained from 90 pancreatic cancer patients and immunohistochemistry studies were performed to determine the integrin αvβ6 expression. After microscopic examination by an experienced pathologist, six samples were excluded from the analysis because they were either detached or contained mostly normal pancreatic tissues. Representative immunohistochemistry staining images of the positive

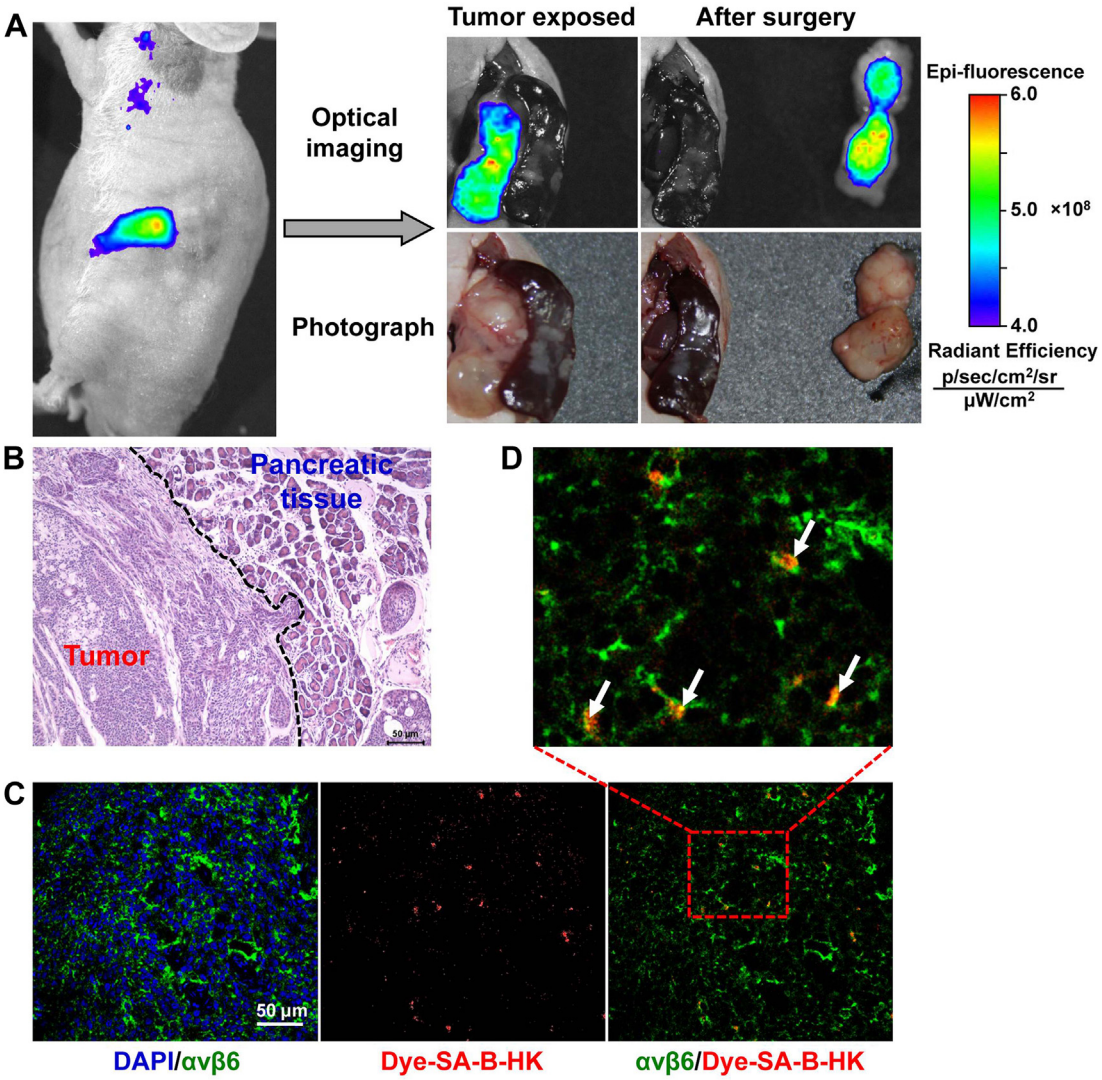

Fig. 3. (A) Near-infrared fluorescence imaging-guided removal of tumors in an orthotopic BxPC-3 pancreatic tumor model at 2 h postinjection of Dye-SA-B-HK. (B) H&E staining of surgically removed tumors. (C) Immunofluorescence staining of human integrin αvβ6 in BxPC-3 tumor tissues harvested from tumor-bearing mice 2 h postinjection of Dye-SA-B-HK. Red color from IRDye700 for Dye-SA-B-HK, green color from FITC for human integrin αvβ6, blue color from DAPI for visualization of nuclei. (D) Magnified images of the boxed areas of C. Arrows indicate the overlaid area. (For interpretation of the references to colour in this figure legend, the reader is referred to the web version of this article.)

and negative stainings are shown in Fig. 6A. By blinded analysis, it was observed that in the remaining 84 samples, 80 were integrin αvβ6-positive whereas 4 samples were integrin αvβ6-negative, resulting in a positivity ratio exceeding 95% (Fig. 6B).

4. Discussion

Cancer-targeted therapy relies on the restricted expression of tumor-specific biomarkers for the selective delivery of therapeutic agents to tumors while sparing normal organs for reduction of the side effects [25]. As one of the most aggressive and extremely malignant tumor types with very poor prognosis, surgical intervention for pancreatic cancer is only possible in 10% of cases, and targeted therapies are generally limited [26]. Previous studies have demonstrated that strong up-regulation of integrin αvβ6 is observed in approximately 100% of pancreatic cancers, whereas it is undetectable or is not expressed in the corresponding normal tissues [16,27]. These findings suggested that integrin αvβ6 is a promising biomarker of pancreatic cancer and potential therapeutic target itself. To validate the overexpression of integrin αvβ6 in tumor tissues of pancreatic cancer patients, we performed a TMA study, which clearly demonstrated that indeed integrin αvβ6 is highly expressed in over 95% cases of a random selected of patient samples (Fig. 6). Thus, overexpression of integrin αvβ6 in pancreatic cancer provides an encouraging rationale for development of integrin αvβ6-targeted agents for potential theranostic application in pancreatic cancer.

In this study, we designed and synthesized an integrin αvβ6-targeted near-infrared fluorescence agent (Dye-SA-B-HK) and investigated it for possible pancreatic cancer-targeted theranostics. The integrin αvβ6-specific peptide HK has been previously demonstrated to be highly specific for integrin αvβ6 and radiolabeled HK peptide can specifically detect integrin αvβ6-expressing tumors [15]. The streptavidin-biotin strategy was used to increase the receptor binding affinity of Dye-SA-B-HK. Although we did not determine the exact binding valence for integrin αvβ6, our cell-competition binding assay clearly demonstrated that the receptor binding affinity of the imaging agent Dye-SA-B-HK was significantly higher than that of the monovalent HK peptide (Fig. 1B). The in vitro high receptor binding affinity of

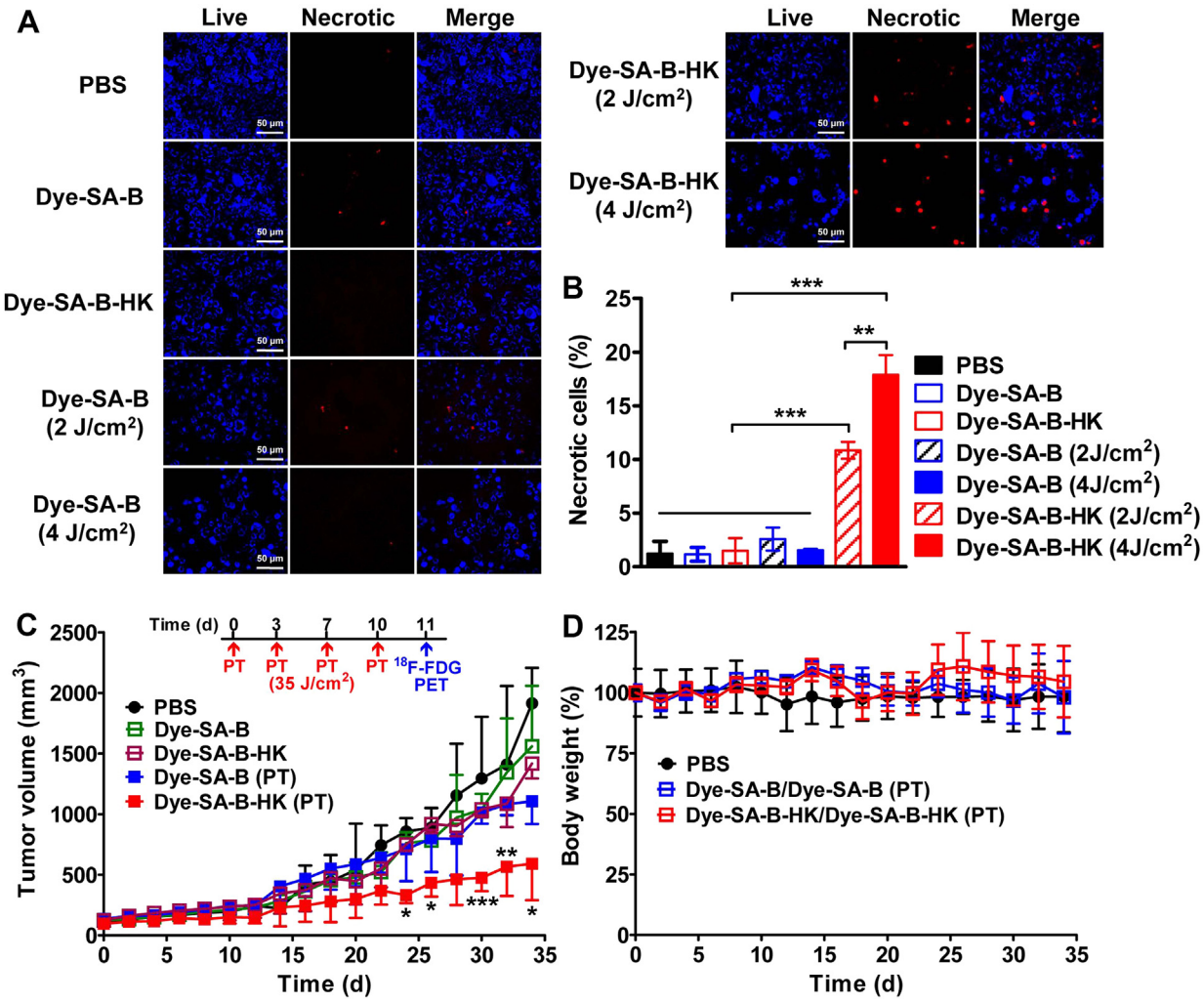

Fig. 4. (A–B) Live and necrotic cell fluorescence staining (A) and quantified fraction of cell necrosis (% necrotic cells) of BxPC-3 tumor cells treated with either PBS, Dye-SA-B, Dye-SA-B-HK, Dye-SA-B (2 or 4 J/cm^2 phototherapy), or Dye-SA-B-HK (2 or 4 J/cm^2 phototherapy). Results are expressed as mean ± SD (n = 5). (C) Growth curves of BxPC-3 tumors in five groups of mice after four-dose treatment with PBS, Dye-SA-B (with or without 35 J/cm^2 phototherapy), or Dye-SA-B-HK (with or without 35 J/cm^2 phototherapy). Results are expressed as mean ± SD (n = 10). Timeline of the phototherapy (PT) and PET imaging experiments are shown above the tumor growth curves. (D) Mean body weight over time in BxPC-3 tumor-bearing nude mice after different treatments (mean ± SD, n = 10). *, $P < 0.05$; **, $P < 0.01$; ***, $P < 0.001$.

Dye-SA-B-HK supported the in vivo application of the NIR fluorescence agent.

The in vivo integrin αvβ6-targeting efficacy of Dye-SA-B-HK was validated using in vivo whole-body fluorescence imaging in the BxPC-3 subcutaneous model. High-contrast tumor targeting of Dye-SA-B-HK was observed and the blocking study and control study using non-targeted Dye-SA-B confirmed the specificity for integrin αvβ6-targeting in vivo. Optical imaging may have limitations in deep tissue imaging and image reconstruction and quantification. However, it can be easily adapted for intraoperative or endoscopic imaging. Therefore, we established an orthotopic pancreatic model that is more clinically relevant. H&E histological examination verified the successful establishment of this mouse model (Fig. 3B). In clinical practice, accurate removal of tumor lesions is crucial for better management of pancreatic cancer to avoid tumor relapse. By using Dye-SA-B-HK optical imaging-guided surgery, tumor lesions can be completely removed, as evidenced by post-surgery optical imaging (Fig. 3A).

Aside from providing guidance for tumor surgery, molecular imaging techniques also play an increasingly important role in the guidance of cancer therapy, including cancer PT [28–30]. The high and specific accumulation of Dye-SA-B-HK suggested its additional application as a cancer phototherapy agent. Thus, we evaluated its potential both in vitro and in vivo. Ideal PT agents should have minimal dark toxicity and are effective in killing cancer cells/tissues under light irradiation [30]. Both in vitro and in vivo data suggested that Dye-SA-B-HK is well tolerated by tumor cells and tumor-bearing nude mice without light irradiation. However, upon light irradiation, effective antitumor effect was observed for Dye-SA-HK, clearly demonstrating the light irradiation-specificity of the PT effect of Dye-SA-HK. BxPC-3 tumor cells treated with Dye-SA-HK phototherapy in vitro had a significantly increased necrosis fraction (Fig. 4A and B), which suggested that the slow tumor growth in the Dye-SA-HK phototherapy group in vivo was caused, at least in part, by tumor cell necrosis.

We used four doses of Dye-SA-B-HK for phototherapy of BxPC-3 tumors and did not observe evident weight loss during the therapy period, suggesting only minor toxicity of this well-tolerated treatment strategy. In previous studies [11,31], the tumor growth curves in the vehicle control groups with or without 690 nm light irradiation were almost identical, demonstrating that light irradiation only with NIR at 690 nm had no effect on tumor growth. In this

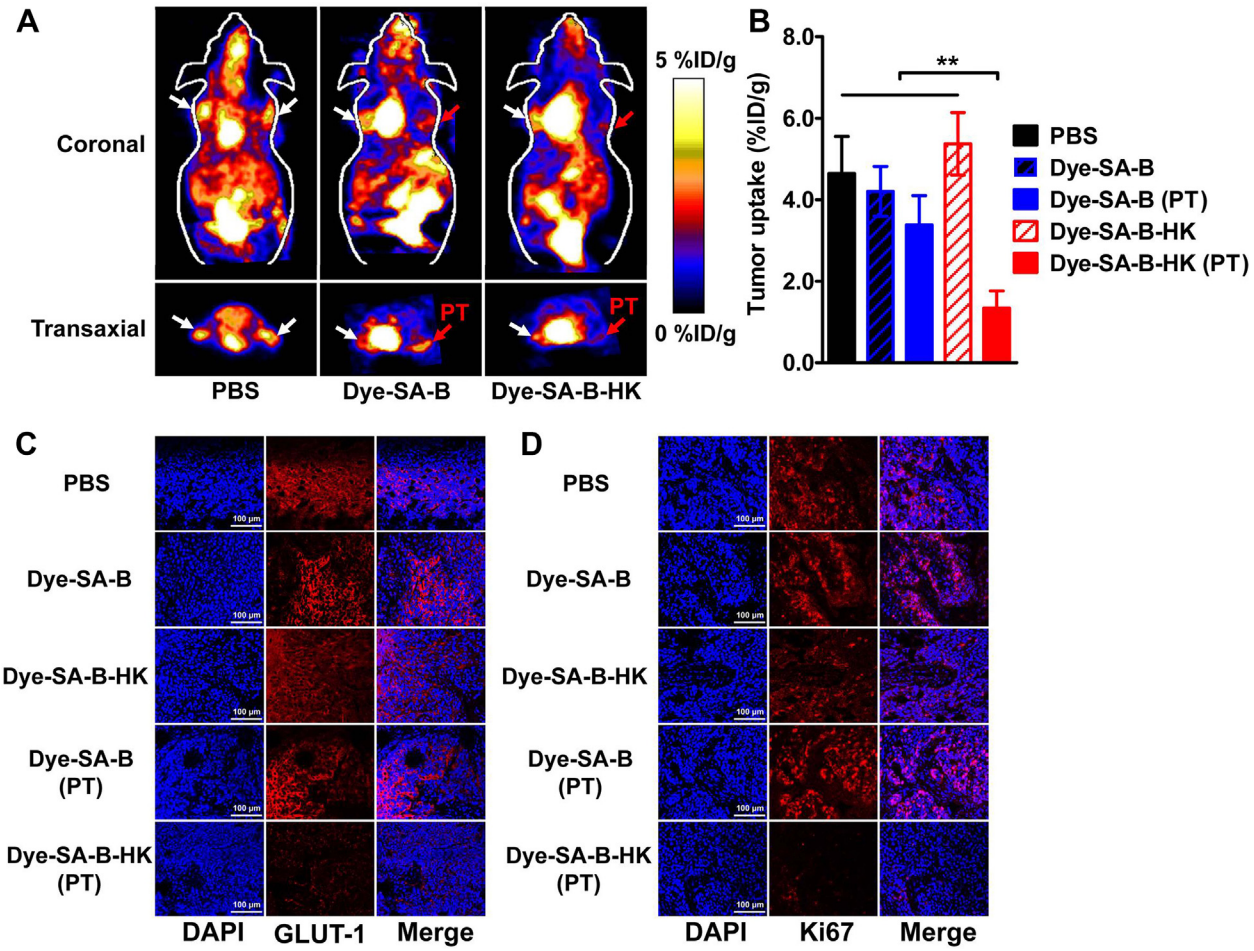

Fig. 5. (A) Decay-corrected whole-body coronal and transaxial small-animal PET images of BxPC-3 tumor-bearing mice 1 h after ^{18}F-FDG injection on day 11 after treatment with PBS, Dye-SA-B (with or without 35 J/cm^2 phototherapy), or Dye-SA-B-HK (with or without 35 J/cm^2 phototherapy). Red and white arrows indicate the tumors with and without phototherapy (PT), respectively. (B) Quantification of tumor uptake from A. Results are expressed as mean ± SD (n = 5). **, $P < 0.01$. (C–D) Immunofluorescence staining of GLUT-1 (C) and Ki67 (D) in BxPC-3 tumor tissues after small-animal PET imaging. (For interpretation of the references to colour in this figure legend, the reader is referred to the web version of this article.)

study, we observed an effective antitumor effect in the Dye-SA-B-HK PT group but not in the non-irradiated groups or the Dye-SA-B PT group. Cancer photodynamic therapy relies on the reactive oxygen species (ROS) for tumor destruction, especially the singlet oxygen (SO) produced by the light irradiated photosensitizer [10,32]. However, SO can only diffuse a very short distance and has a short half-life [33,34]. Therefore, the receptor recognition in the tumor tissues is needed to effect delivery of the photosensitizer to the tumor cell surface, thereby generating effective antitumor effect. This may explain that although Dye-SA-B had non-specific uptake in the tumor (Fig. 2D and E) due to the enhanced permeability and retention (EPR) effect [35], we did not observed evident tumor suppression effect for Dye-SA-B upon light irradiation (Fig. 4C).

Our in vivo small-animal whole body ^{18}F-FDG PET imaging manifested a remarkable decrease in ^{18}F-FDG tumor uptake in the Dye-SA-B-HK PT group compared with the control groups on day 11 after treatment (Fig. 5A and B). Note that at this time point, no change in tumor size was observed (Fig. 4C). The visualized tumor responses by ^{18}F-FDG PET imaging preceded the statistically significant decrease observed in tumor size (day 24; Fig. 4C) by at least 13 days. These results demonstrate the sensitivity of ^{18}F-FDG PET imaging in the identification of early tumor responses to Dye-SA-B-HK phototherapy. To validate the results of ^{18}F-FDG PET imaging in vivo, we performed ex vivo immunofluorescence staining of GLUT-1, a marker reflecting tumor glucose metabolism. Since Ki67 level reflects cell proliferation index, we also stained the tumor tissues for Ki67 to validate the in vivo antitumor effect of Dye-SA-B-HK phototherapy. Ex vivo staining results revealed decreased glucose activity and a lower proliferative index in Dye-SA-B-HK PT-treated tumors, which confirmed the in vivo ^{18}F-FDG PET imaging results.

This study demonstrated the potential use of streptavidin-biotin chemistry with easily self-assembly for the generation of a tumor-targeting agent for simultaneously theranostic application for cancer treatment. Streptavidin modification for labeling of imaging tags (e.g., radioisotopes for PET and SPECT; fluorescence dyes for optical imaging) did not affect the tumor-targeting efficacy of the imaging agents (the targeting motif of the imaging agents was conjugated to biotin but not streptavidin). Therefore, a dual or multi-functional molecular imaging agent composed of both a radioisotope and a near-infrared phthalocyanine dye labeled on the streptavidin could also be easily synthesized without affecting receptor binding. With this imaging agent, the location of primary and metastatic tumor lesions can be identified by initial whole-body PET or SPECT scan. Subsequently the tumor surgery and phototherapy can then be performed under optical imaging guidance. Note that in the present study, we used human pancreatic

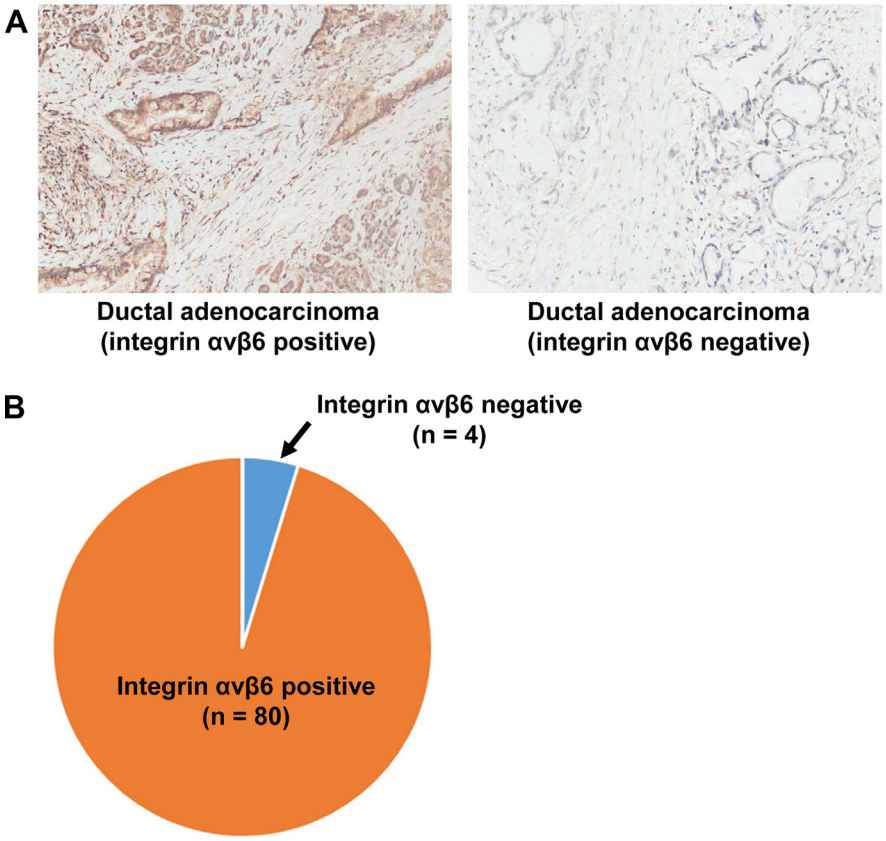

Fig. 6. (A) Representative immunohistochemistry staining images of the positive and negative staining for integrin αvβ6 in human pancreatic cancer tissue microarrays. (B) The pie graph showed that in the 84 samples examined, 80 were integrin αvβ6 positive whereas 4 samples were integrin αvβ6 negative, a positive ratio of 95.24%.

cancer xenograft mouse models established by inoculating human cancer cells into the mice, which cannot fully mimic the clinical situation. Future studies using a patient derived xenograft (PDX) model or a transgenic pancreatic cancer model may be needed to further illustrate the potential of Dye-SA-B-HK for clinical use.

5. Conclusion

We prepared and evaluated an integrin αvβ6-targeting near-infrared agent Dye-SA-B-HK for in vivo imaging, guided surgery and phototherapy in pancreatic cancer mouse models. Dye-SA-B-HK exhibited specific integrin αvβ6-targeting both in vitro and in vivo. In an orthotopic pancreatic mouse model, Dye-SA-B-HK was successfully applied for optical image-guided removal of tumor lesions. By external light irradiation, a remarkable antitumor effect of Dye-SA-B-HK was observed and the tumor therapy responses were validated by small-animal PET imaging and ex vivo fluorescence staining. Taken together, Dye-SA-B-HK is a promising agent for theranostics of integrin αvβ6-expressing malignances, including pancreatic cancer.

Acknowledgments

This work was supported, in part, by National Natural Science Foundation of China (NSFC) projects (81471712, 81222019, 81125011, and 81371614), “973” projects (2013CB733802 and 2011CB707705), grants from the Ministry of Science and Technology of China (2011YQ030114, 2012ZX09102301, and 2012BAK25B03), grants from Beijing Natural Science Foundation (7132131 and 7132123), and a grant from the Beijing Nova Program (Z121107002512010).

References

[1] Vincent A, Herman J, Schulick R, Hruban RH, Goggins M. Pancreatic cancer. Lancet 2011;378:607–20.
[2] Stathis A, Moore MJ. Advanced pancreatic carcinoma: current treatment and future challenges. Nat Rev Clin Oncol 2010;7:163–72.
[3] Hidalgo M. Pancreatic cancer. N Engl J Med 2010;362:1605–17.
[4] van Dam GM, Themelis G, Crane LM, Harlaar NJ, Pleijhuis RG, Kelder W, et al. Intraoperative tumor-specific fluorescence imaging in ovarian cancer by folate receptor-alpha targeting: first in-human results. Nat Med 2011;17:1315–9.
[5] Weissleder R, Ntziachristos V. Shedding light onto live molecular targets. Nat Med 2003;9:123–8.
[6] Ntziachristos V, Bremer C, Weissleder R. Fluorescence imaging with near-infrared light: new technological advances that enable in vivo molecular imaging. Eur Radiol 2003;13:195–208.
[7] Yuan A, Wu J, Tang X, Zhao L, Xu F, Hu Y. Application of near-infrared dyes for tumor imaging, photothermal, and photodynamic therapies. J Pharm Sci 2013;102:6–28.
[8] Agostinis P, Berg K, Cengel KA, Foster TH, Girotti AW, Gollnick SO, et al. Photodynamic therapy of cancer: an update. CA Cancer J Clin 2011;61:250–81.
[9] Cheng L, Wang C, Feng L, Yang K, Liu Z. Functional nanomaterials for phototherapies of cancer. Chem Rev 2014;114:10869–939.
[10] Triesscheijn M, Baas P, Schellens JH, Stewart FA. Photodynamic therapy in oncology. Oncologist 2006;11:1034–44.
[11] Mitsunaga M, Ogawa M, Kosaka N, Rosenblum LT, Choyke PL, Kobayashi H. Cancer cell-selective in vivo near infrared photoimmunotherapy targeting specific membrane molecules. Nat Med 2011;17:1685–91.
[12] Nakajima T, Sano K, Choyke PL, Kobayashi H. Improving the efficacy of Photoimmunotherapy (PIT) using a cocktail of antibody conjugates in a multiple antigen tumor model. Theranostics 2013;3:357–65.
[13] Sano K, Mitsunaga M, Nakajima T, Choyke PL, Kobayashi H. Acute cytotoxic effects of photoimmunotherapy assessed by ^{18}F-FDG PET. J Nucl Med 2013;54:770–5.

[14] Wu AM, Olafsen T. Antibodies for molecular imaging of cancer. Cancer J 2008;14:191–7.
[15] Liu Z, Liu H, Ma T, Sun X, Shi J, Jia B, et al. Integrin alphavbeta6-targeted SPECT imaging for pancreatic cancer detection. J Nucl Med 2014;55:989–94.
[16] Bandyopadhyay A, Raghavan S. Defining the role of integrin alphavbeta6 in cancer. Curr Drug Targets 2009;10:645–52.
[17] Liu H, Wu Y, Wang F, Liu Z. Molecular imaging of integrin alphavbeta6 expression in living subjects. Am J Nucl Med Mol Imaging 2014;4:333–45.
[18] Oyama T, Sykes KF, Samli KN, Minna JD, Johnston SA, Brown KC. Isolation of lung tumor specific peptides from a random peptide library: generation of diagnostic and cell-targeting reagents. Cancer Lett 2003;202:219–30.
[19] Liu Z, Sun X, Liu H, Ma T, Shi J, Jia B, et al. Early assessment of tumor response to gefitinib treatment by noninvasive optical imaging of tumor vascular endothelial growth factor expression in animal models. J Nucl Med 2014;55:818–23.
[20] Sun X, Ma T, Liu H, Yu X, Wu Y, Shi J, et al. Longitudinal monitoring of tumor antiangiogenic therapy with near-infrared fluorophore-labeled agents targeted to integrin alphavbeta3 and vascular endothelial growth factor. Eur J Nucl Med Mol Imaging 2014;41:1428–39.
[21] Liu Z, Yu Z, He W, Ma S, Sun L, Wang F. In-vitro internalization and in-vivo tumor uptake of anti-EGFR monoclonal antibody LA22 in A549 lung cancer cells and animal model. Cancer Biother Radiopharm 2009;24:15–24.
[22] Liu Z, Huang J, Dong C, Cui L, Jin X, Jia B, et al. ^{99m}Tc-labeled RGD-BBN peptide for small-animal SPECT/CT of lung carcinoma. Mol Pharmacol 2012;9:1409–17.
[23] Zhu XD, Zhang JB, Zhuang PY, Zhu HG, Zhang W, Xiong YQ, et al. High expression of macrophage colony-stimulating factor in peritumoral liver tissue is associated with poor survival after curative resection of hepatocellular carcinoma. J Clin Oncol 2008;26:2707–16.
[24] Elayadi AN, Samli KN, Prudkin L, Liu YH, Bian A, Xie XJ, et al. A peptide selected by biopanning identifies the integrin alphavbeta6 as a prognostic biomarker for nonsmall cell lung cancer. Cancer Res 2007;67:5889–95.
[25] Ersahin D, Doddamane I, Cheng D. Targeted radionuclide therapy. Cancers – Basel 2011;3:3838–55.
[26] Singh P, Srinivasan R, Wig JD. Major molecular markers in pancreatic ductal adenocarcinoma and their roles in screening, diagnosis, prognosis, and treatment. Pancreas 2011;40:644–52.
[27] Sipos B, Hahn D, Carceller A, Piulats J, Hedderich J, Kalthoff H, et al. Immunohistochemical screening for beta6-integrin subunit expression in adenocarcinomas using a novel monoclonal antibody reveals strong up-regulation in pancreatic ductal adenocarcinomas in vivo and in vitro. Histopathology 2004;45:226–36.
[28] Guo M, Mao H, Li Y, Zhu A, He H, Yang H, et al. Dual imaging-guided photothermal/photodynamic therapy using micelles. Biomaterials 2014;35:4656–66.
[29] Haedicke K, Grafe S, Lehmann F, Hilger I. Multiplexed in vivo fluorescence optical imaging of the therapeutic efficacy of photodynamic therapy. Biomaterials 2013;34:10075–83.
[30] Rong P, Yang K, Srivastan A, Kiesewetter DO, Yue X, Wang F, et al. Photosensitizer loaded nano-graphene for multimodality imaging guided tumor photodynamic therapy. Theranostics 2014;4:229–39.
[31] Mitsunaga M, Nakajima T, Sano K, Choyke PL, Kobayashi H. Near-infrared theranostic photoimmunotherapy (PIT): repeated exposure of light enhances the effect of immunoconjugate. Bioconj Chem 2012;23:604–9.
[32] Dolmans DE, Fukumura D, Jain RK. Photodynamic therapy for cancer. Nat Rev Cancer 2003;3:380–7.
[33] Yoo JO, Ha KS. New insights into the mechanisms for photodynamic therapy-induced cancer cell death. Int Rev Cell Mol Biol 2012;295:139–74.
[34] Shirasu N, Yamada H, Shibaguchi H, Kuroki M, Kuroki M. Potent and specific antitumor effect of CEA-targeted photoimmunotherapy. Int J Cancer 2014;135:2697–710.
[35] Maeda H, Fang J, Inutsuka T, Kitamoto Y. Vascular permeability enhancement in solid tumor: various factors, mechanisms involved and its implications. Int Immunopharmacol 2003;3:319–28.